ELSEVIER

Contents lists available at ScienceDirect

Electrochimica Acta

journal homepage: www.journals.elsevier.com/electrochimica-acta



The role of nonmetallic ion substitution in perovskite LaCoO₃ for improved oxygen evolution reaction activity

Maoyu Wang ^{a,b,1}, Kingsley Chukwuma Chukwu ^{a,1}, Brian A. Muhich ^a, Widitha S. Samarakoon ^{a,c}, Zizhou He ^d, Marcos Lucero ^a, Chun-Wai Chang ^a, Alvin Chang ^a, Dongqi Yang ^a, Sumandeep Kaur ^a, Alpha T. N'Diaye ^e, George E. Sterbinsky ^b, Yingge Du ^c, Ling Fei ^d, Líney Árnadóttir ^{a,*}, Zhenxing Feng ^{a,*}

- a Department of Chemical, Biological and Environmental Engineering, Oregon State University, Corvallis, OR 97331, United States
- ^b Advanced Photon Source, Argonne National Laboratory, Lemont, IL 60439, United States
- ^c Physical and Computational Sciences Directorate, Pacific Northwest National Laboratory, Richland, WA 99354, United States
- ^d Chemical Engineering Department, University of Louisiana at Lafayette, Lafayette, LA 70504, United States
- ^e Advanced Light Source, Lawrence Berkeley National Laboratory, Berkeley, CA 94720, United States

ARTICLE INFO

Keywords: Oxygen evolution reaction Electronic structure Property descriptor In-situ X-ray absorption spectroscopy

ABSTRACT

Transition metal perovskite (ABO₃) is an emerging type of oxygen evolution reaction (OER) electrocatalyst that shows reasonably good activity and moderate stability. Although efforts have been made to improve perovskite' OER performance by various element substitution at A/B-site, the influence of ion, particularly non-metallic ion, substitutions on the OER mechanism are rarely studied. More and more evidence has shown that the metal-center theory has failed to explain lots of OER-related phenomena. Therefore, it is urgent to understand how the cation and anion sites in perovskite determine OER performance. Here, we used a Fe and P co-doped LaCoO₃ as a model system to explore the influence of substitution in perovskite by combining operando/ex-situ X-ray characterization and density functional theroy (DFT). We observed enhanced OER catalytic activities in co-doped materials, which are attributed to the stronger transition-metal-oxygen-bonding-covalency (TMOBC). The detailed analyses by O K-edge XAS, electrochemical performance, and DFT suggest that the hybridization between O 2p and transition metal 3d e_g orbitals could be a more credible descriptor of perovskite for OER, which is the combination of e_g orbital theory and TMOBC theory. The finding in our work provides insights into the OER catalysis mechanism on metal oxides, which could guide new design of cost-effective oxide electrocatalysts.

1. Introduction

Developing sustainable energy conversion and storage techniques is key to combatting climate change and responding to its harmful effects [1–3]. A promising solution is the use of electrochemical energy conversion devices such as electrolyzes to split water and produce hydrogen, which can be stored and used as a green energy resource, thereby promoting the so-called "hydrogen economy" [4,5]. Water splitting consists of two main electrochemical reactions, namely hydrogen evolution reaction (HER) and oxygen evolution reaction (OER), occurring at the cathode and the anode, respectively., The OER is a four-electron process that is more challenging, compared to HER, due to its relatively sluggish kinetics and high overpotential [6,7].

Therefore, significant emphasis has been directed towards conducting research to identify cost-effective, active, and stable electrocatalysts for promoting OER.

Over the past decades, efficient OER catalysts have been mainly based on precious metals and their oxides such as IrO_2 and RuO_2 . Due to their high costs, alternative materials such as transition metal oxides have been explored as electrocatalysts for OER. For example, Shao-Horn's group has shown that $Ba_{0.5}Sr_{0.5}Co_{0.8}Fe_{0.2}O_{3-\delta}$ has much better catalytic activity than the state-of-the-art IrO_2 [8]. They also pointed out that the highest OER activity could be achieved when the electron occupancy of the metal e_g orbital is close to unity [8]. Based on the e_g orbit theory, Xu's group tailored the Co-O bonding covalency via substituting Fe with Co in LaCoO₃ [7]. They found that $LaCo_{0.9}Fe_{0.1}O_3$ exhibits the

^{*} Corresponding authors.

E-mail addresses: Liney.Arnadottir@oregonstate.edu (L. Árnadóttir), zhenxing.feng@oregonstate.edu (Z. Feng).

¹ These authors contributed equally to this work.

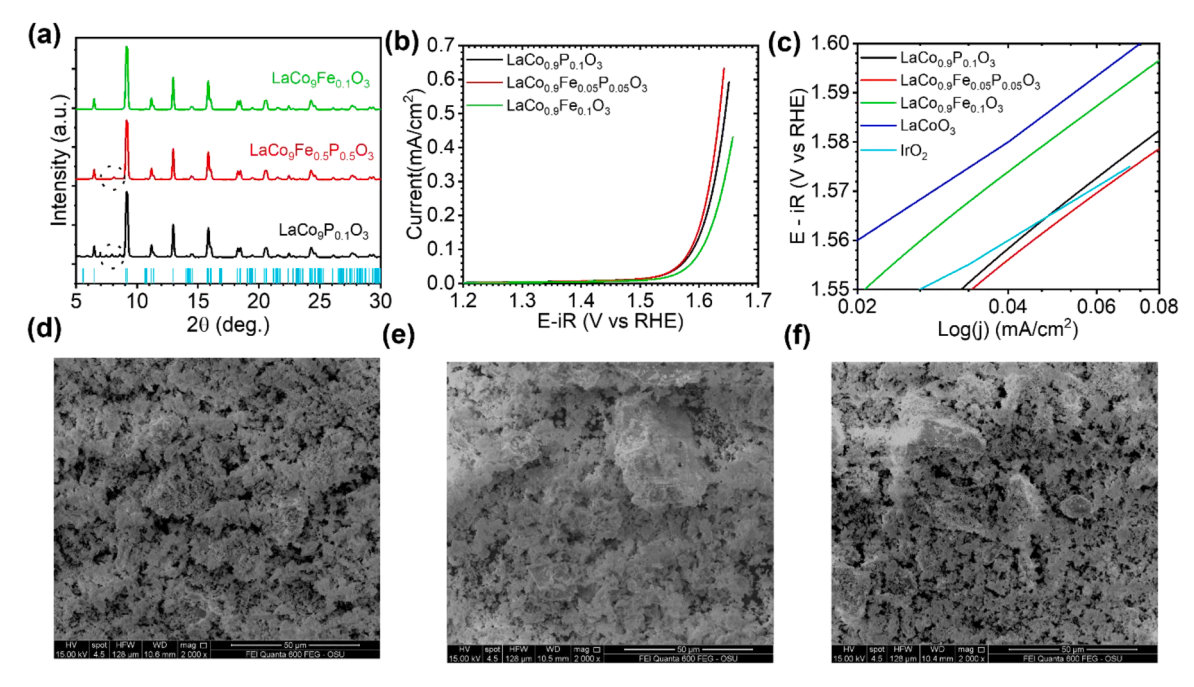


Fig. 1. (a) XRD diffraction with LaCoO $_3$ standard at bottom (b) OER performance of LaCo $_0.9$ P $_0.1$ O $_3$, LaCo $_0.9$ Fe $_0.05$ O $_3$, and LaCo $_0.9$ Fe $_0.1$ O $_3$ (c) Tafel plot of different peroxides compared with unsubstituted LaCoO $_3$ extracted from Ref 7 and benchmarked IrO $_2$ extracted from Ref 11; SEM of (d) LaCo $_0.9$ P $_0.1$ O $_3$, (e) LaCo $_0.9$ Fe $_0.05$ O $_3$, and (f) LaCo $_0.9$ Fe $_0.05$ O $_3$, and (f) LaCo $_0.9$ Fe $_0.1$ O $_3$.

best OER performance among different percentages of Fe substitution due to the highest transition-metal-oxygen-bonding covalency (TMOBC) [6]. Recently, the P substitution has been explored as an alternative approach to enhance the OER performance of perovskites [9,10]. For example, Chen's group found that the high-valence-state P substitution in SrCo_{0.8}Fe_{0.2}O₃ enhances the OER performance, which is attributed to the introduction of more oxygen vacancies. Different from metal substitution, P substitution in perovskite oxides provides a non-metallic site. This challenges the metal-centered theory (e.g., e_g orbital theory) and requires more fundamental understanding of the influence of anion substitution, or more generally the role of cation and anion substitution

in perovskite oxides electrocatalysts.

In this work, we substituted Fe and P into $LaCoO_3$ to understand the role of cation and anion doping such as whether P could adjust TMOBC similar to Fe. This is the extension of the previous work on Fe doping in $LaCoO_3$ [7]. The electrochemical performance indicates the P doping could improve the OER catalytic performance, and Tafel slope suggested that P doping does not change the reaction mechanism. With the help of multimodal characterization tools including *operando* X-ray diffraction (XRD) and *operando* hard X-ray absorption spectroscopy (XAS) together with electrochemical performance, we revealed that those materials, particularly the metal sites, did not undergo any obvious crystal and

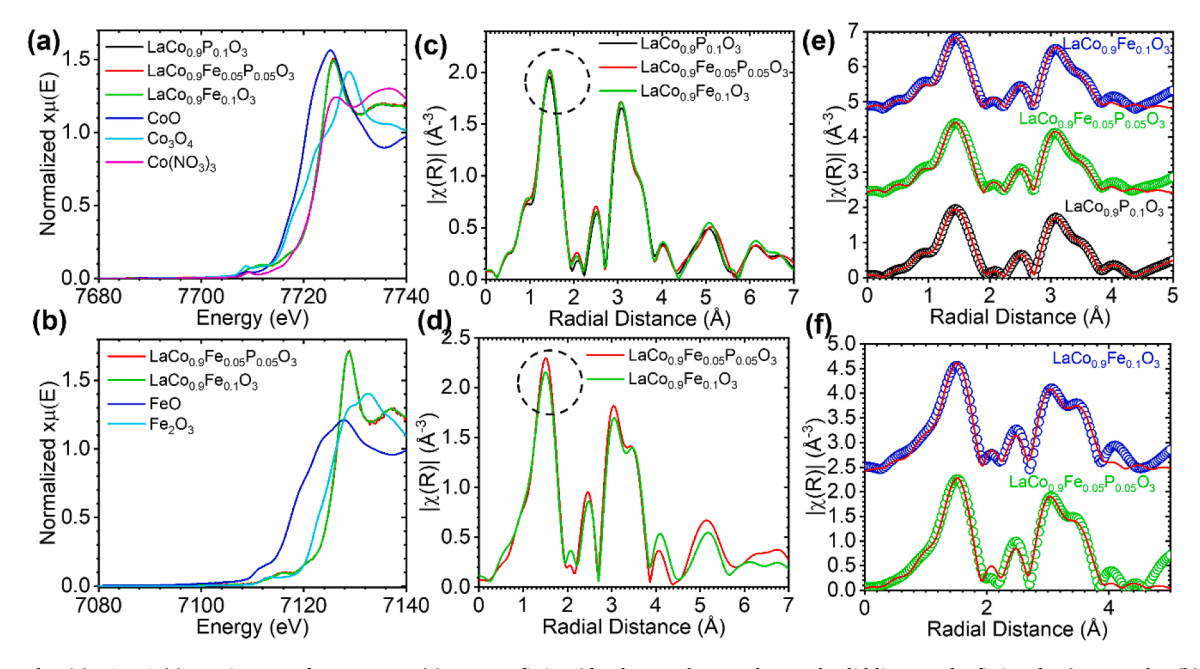
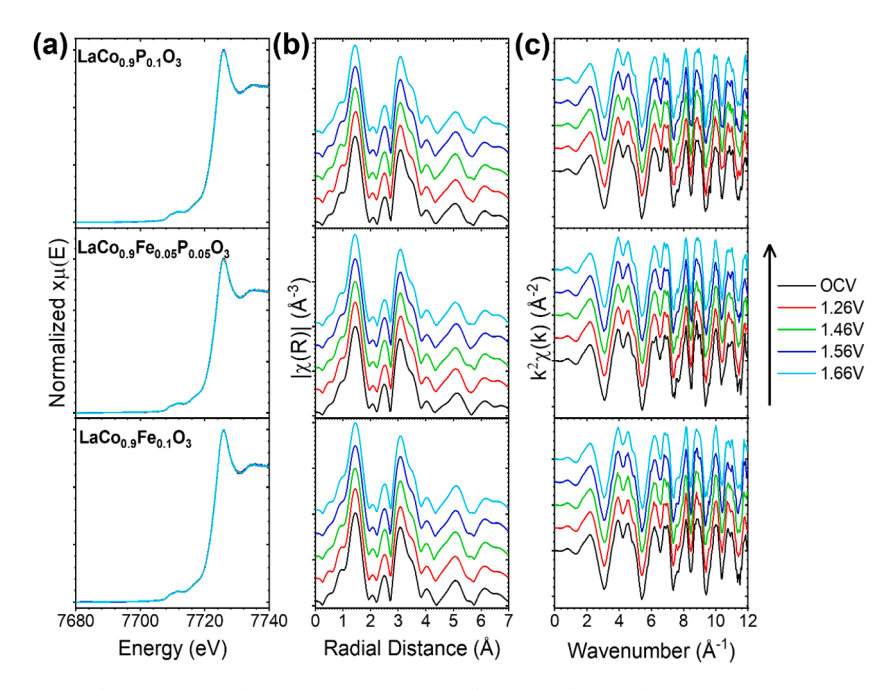


Fig. 2. Co K-edge (a) XANES (c) Fourier Transform R-space (e) R-space fitting (the dot are the raw data and solid line are the fitting data); Fe K-edge (b) XANES (d) Fourier Transform R-space (f) R-space fitting (the dot are the raw data and solid line are the fitting data) of LaCo_{0.9}Po_{0.1}O₃, LaCo_{0.9}Fe_{0.05}Po_{0.05}O₃, and LaCo_{0.9}Fe_{0.1}O₃.



 $\textbf{Fig. 3.} \ \ \textit{Operando} \ \ \textit{Co} \ \ \textit{K-edge} \ \ \textbf{(a)} \ \ \textit{XANES} \ \ \textbf{(b)} \ \ \textit{Fourier Transfer EXAFS} \ \ \textit{in R-space} \ \ \textbf{(c)} \ \ \textit{and EXAFS} \ \ \textit{in k-space for LaCo}_{0.9}P_{0.1}O_3, \ \ \textit{LaCo}_{0.9}F_{0.05}P_{0.05}O_3, \ \ \textit{and LaCo}_{0.9}F_{0.1}O_3.$

local structure changes under OER conditions, which suggests that the cation may not be the only reaction center. Furthermore, $ex\hbox{-}situ$ soft XAS illustrated that P substitution did not change neither Co nor Fe electronic structure or crystal structure but did change TMOBC. Therefore, by combining O K-edge XAS with the density functional theory (DFT) analysis, we provided a new way to explain the enhanced OER performance: the hybridization between e_g orbitals and O 2p orbitals is more critical to determine the OER performance in oxide electrocatalysts.

2. Results and discussion

XRD was carried out to reveal the crystal structure of LaCo_{0.9}P_{0.1}O₃, LaCo_{0.9}Fe_{0.05}P_{0.05}O₃, and LaCo_{0.9}Fe_{0.1}O₃ (Fig. 1a). All three materials show the rhombohedral structure, which is the same as pure LaCoO3 and there is no phase transition change caused by Fe and P substitution. Rietveld refinement was carried out to further confirm the lattice parameter change (Fig. S1 & Table S1). There are some small lattice changes of the three materials which may be caused by the Fe and P doping. In addition, some low-angle peaks were missing in LaCo_{0.9}P_{0.1}O₃ and LaCo_{0.95}Fe_{0.05}P_{0.05}O₃ from the refinement when using the LaCoO₃ crystal structure. This indicates the P doping of B-site as suggested in the previous study [9-11]. To quantify the surface area of $LaCo_{0.9}Fe_xP_{0.1-x}O_3$, the Brunauer-Emmett-Teller (BET) tests were carried out and the specific surface areas of these LaCo_{0.9}Fe_xP_{0.1-x}O₃ were measured to be around 3.6 \mbox{m}^2/\mbox{g} (Table S2). Scanning electron microscopy (Fig. 1d-f) confirms that all those materials have similar morphology. Energy dispersive spectroscopy (EDS) was also carried out to ensure that we successfully substituted Fe and P into the LaCoO3 (Fig. S2). The element distribution ratio estimated from EDS (Table S3) confirms the expected composition of the synthesized materials. By carefully estimating the atomic ratio of Fe, Co, and P with La, it suggests that $LaCo_{0.9}Fe_{0.05}P_{0.05}O_3$ has around half amount of P compared with LaCo_{0.9}P_{0.1}O₃ and half the amount of Fe compared with LaCo_{0.9}Fe_{0.1}O₃. This also confirms the P and Fe doping in B-site [11]. The OER performance of LaCo_{0.9}Fe_xP_{0.1-x}O₃ was tested in 0.1 M KOH solutions using the three-electrode rotating disk method. The OER current normalized with the BET surface area indicates that LaCo_{0.9}Fe_{0.05}P_{0.05}O₃ has the best OER performance (Fig. 1b) with the lowest onset potential (i.e., 1.60 V at 0.2 mA/cm²), and the LaCo_{0.9}Fe_{0.1}O₃ shows the worst OER performance (i.e., 1.63 V at 0.2 mA/cm²). Note that our LaCo_{0.9}Fe_{0.1}O₃

exhibits the same OER performance as described in previous literature (i.e., 1.63 V at 0.2 mA/cm^2) [7], which confirms that our P-substitution further enhances the OER catalytic activity, but still little worse than standard RuO₂ (Fig. S3). The better OER activity of Fe and P doped oxides in our study is also reflected by the comparison of Tafel slopes of our samples with those reported in literature, including IrO₂ (Fig. 1c) [7, 12]. However, the slope of Tafel plots are very close around four materials, which indicates the similar reaction mechanism or reaction pathway. Hence, the difference between catalytic performance is more likely related to materials' intrinsic characteristic parameters.

Ex-situ XAS was carried out to obtain the valence state, electronic structure, and local structure of both Co and Fe (Fig. 2a&b) [13-16]. Although the shapes of X-ray absorption near edge structure (XANES) spectra of our electrocatalysts are different from Co(NO₃)₃ and Fe₂O₃ due to different local structures of perovskites and standards (Fig. 2a&b), all three $LaCo_{0.9}Fe_xP_{0.1-x}O_3$ show the same Co and Fe valence states with Co valence state close to Co(III) and Fe with slightly higher valence state than Fe(III) [7,13], which suggests that the substitution does not change the oxidization state to influence the OER performance. Note that a minor spectra difference (highlighted by circles in Fig. 2e&f) on extended X-ray absorption fine structure (EXAFS) of Fe and Co may be caused by the Fourier transformation of the noise in the k-space (Fig. S4) or the actual oxygen vacancy. Since the oxygen vacancy would also plays a critical role in the OER catalytic performance, we carried the model based (LaCoO3 as the study model) EXAFS fitting to estimate the oxygen coordination with both Co and Fe (Fig. 2e, f &S5). Based on the EXAFS fitting results (Table S4&5), there is only tiny Co-O/Fe-O coordination number difference three samples. Considering the error bar, those slight differences may be caused by the noise point in the k-space or some small amount of oxygen vacancies formation on the surface due to P doping. However, the amount of oxygen vacancies are not significant, which do not play a crital role in the OER performance. Hence, the P substitution does not induce different OER performance through alteration of the metal oxidization state or local structure.

To further understand the OER reaction mechanism and how P-substitution is achieved, the *operando* characterizations under catalytic reaction were carried out. *Operando* XRD (Fig. S6) showed no change in the bulk crystal structure for all three materials, which confirms that the OER only takes place on the surface of the materials. *Operando* XAS

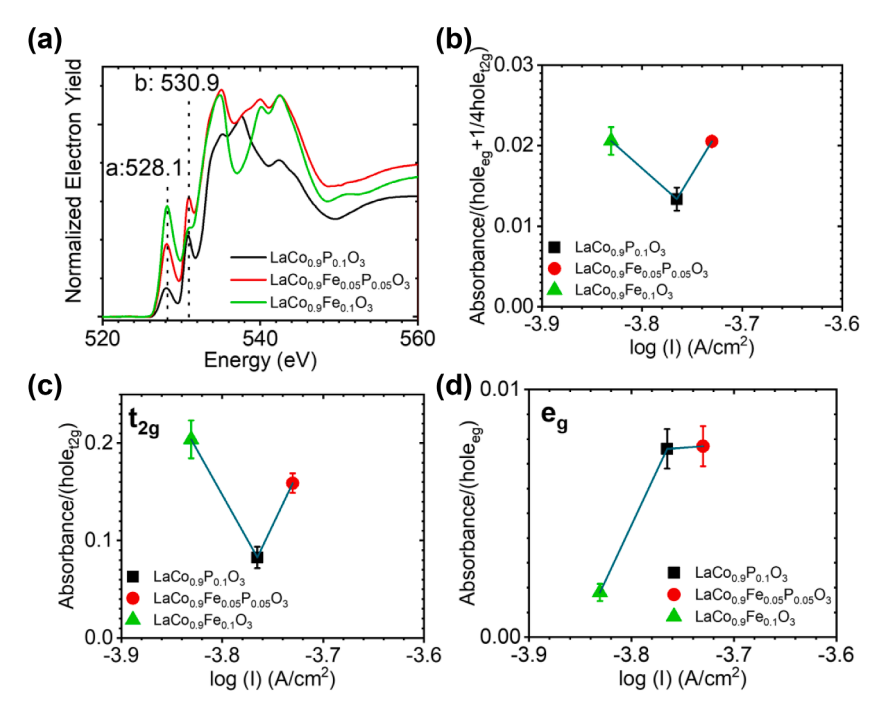


Fig. 4. (a) O K-edge XAS, (b) estimated TMOBC based on the total area of peaks a and b, (c) estimated transition metal t_{2g} and O 2p hybridization based on the area of peak a, (d) estimated transition metal e_g and O 2p hybridization based on the area of peak b for LaCo_{0.9}P_{0.1}O₃, LaCo_{0.9}Fe_{0.05}P_{0.05}O₃, and LaCo_{0.9}Fe_{0.1}O₃ (The current density for comparing is the current at overpotential equaling to 0.3 V).

measurements were also carried out to probe any electronic structure or local structure change during the OER (Fig. 3&S7) [17,18]. Based on the Co K-edge XANES, there is no Co electronic structure change in the LaCo_{0.9}Fe_xP_{0.1-x}O₃ materials during the catalytic reaction (Fig. 3a). In addition, no change in Co local structure of the LaCo_{0.9}Fe_xP_{0.1-x}O₃ materials was observed (Fig. 3b&c). The operando Fe K-edge XAS measurements (Fig. S7) provide similar results. These results showed no electronic or local structure changes in the materials during the catalytic reaction. Note that XAS is a bulk-sensitive technique. Since most of the bulk Co and Fe are not involved in the reaction, changes in the surface Co and Fe could be below the XAS detection limit [19]. In addition, a previous study used a surface-sensitive hard XAS to indicate only a small amount of LaCoO3 on the surface undergoes catalytic reaction [20]. It is also possible that the bulk oxygen is involved in the catalytic reaction, which may not cause any structure change of Co and Fe [21]. Therefore, the surface sensitive ex-situ soft XAS at Fe L-edge and Co L-edge were also carried out to probe the surface Fe oxidization state and the electronic structure using electron yield mode [16]. Although there is slightly difference in L3 peak of both Co and Fe for all electrocatalysts, but the peak location and distribution are the same around three materials, (Fig. S8), which indicates the almost same surface oxidization state (Co(III) and Fe(III)) and electronic structure [22-27].

As no electronic structure and local structure changes were identified at the cation site, the e_g orbital theory based on 3d transition metal does not work well to explain the increased OER performance of the $LaCo_{0.9}Fe_xP_{0.1-x}O_3$ materials. Therefore, the TMOBC theory, another important descriptor for perovskite OER performance [7,8], was performance. considered to explain the electrocatalytic Surface-sensitive O K-edge XAS measurements were carried out to estimate the TMOBC (Fig. 4a) [27–30]. The P substitution has a significant influence on the O K-edge spectrum. Fig. 4a shows peak a and peak b can be used to estimate the TMOBC. Their changes emphasize the difference in metal-oxygen covalency of the three LaCo_{0.9}Fe_xP_{0.1-x}O₃ materials, which could explain the different OER catalytic activities. The areas of peak a and peak b were further analyzed to quantify the strength of TMOBC. Based on the method mentioned in previous literature[22,30] and our soft XAS study [27], Co and Fe were treated as Co(III) with

intermediate spin and Fe(III) with high spin, respectively, based on the Co and Fe L-edge soft XAS data (Fig. S8) and their similarities in spectra shapes reported in literature [7,8,22,24,26,27]. The results (Fig. 4b) illustrate that LaCo_{0.9}Fe_{0.05}P_{0.05}O₃ has the strongest TMOBC, which can be correlated to the best OER performance among the three materials and is consistent with previous reported trend [7,22]. However, the LaCo_{0.9}Fe_{0.1}O₃ that exhibited worse OER performance than LaCo_{0.9}P_{0.1}O₃ showed stronger TMOBC strength. This opposite trend suggests that more detailed analysis or alternative theory is needed. When transition metal cations are involved in adsorption, desorption and formation of a surface chemical bonds of the reaction intermediates, the materials' chemical properties are mainly determined by the outermost antibonding orbital 3d e $_g$ while 3d t $_{2g}$ is less involved. Thus, the hybridization of the transition metal $3d e_g$ and the oxygen 2p is more influential in electrocatalysts' activity than that of the transition metal $3d t_{2g}$ and the oxygen 2p. For O K-edge XAS spectrum, peak a reflects the transition metal t_{2g} and O 2p hybridization and peak b can be treated as the transition metal e_g and O 2p hybridization [28]. Their estimated hybridizations are shown in Fig. 4c and d, respectively. Clearly, the trend of TMOBC strength shown in Fig. 4d matches that of the OER activity of the three electrocatalysts, suggesting that the hybridization between metal eg and oxygen 2p is the dominate factor. Comparatively, the TMOBC strength in Fig. 4c, which reflects the metal t_{2g} and O 2p hybridization, fails to explain the three electrocatalysts' OER activity. Hence, we propose a new descriptor for perovskite OER catalytic performance: the greater transition metal e_g orbital hybridization with O 2porbital leads to higher OER performance.

In alkaline media, the widely accepted OER mechanism on metal oxides consists of the following four-electron/proton transfer steps [31–34]:

```
Step 1: OH^- + * \rightarrow OH^* + e^-
Step 2: OH^* + OH^- \rightarrow O^* + H_2O + e^-
Step 3: O^* + OH^- \rightarrow OOH^* + e^-
Step 4: OOH^* + OH^- \rightarrow * + O_2 + H_2O + e^-
```

The first step describes a hydroxyl radical adsorbed on the active site (*) to give OH* by 1 e $^-$ oxidation of hydroxide anion (OH $^-$). Then the coupled proton and electron removal from OH* leads to O* in the second

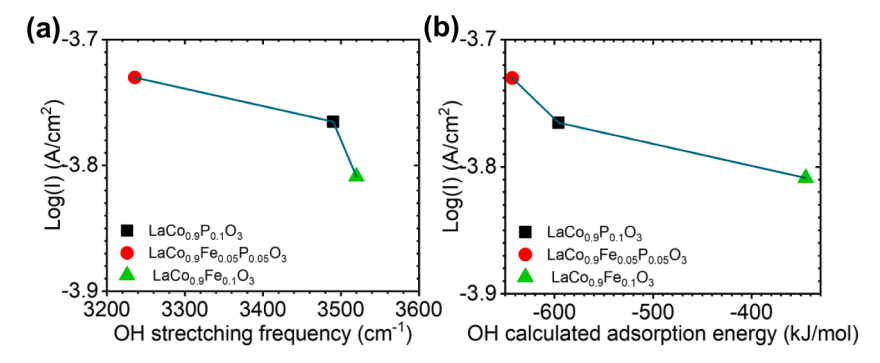


Fig. 5. (a) Plot of the log of the experimental current density (at 0.3 V overpotential) vs DFT stretching frequency of OH on different Perovskite structure (b) Plot of the log of the experimental current density (at 0.3 V overpotential) vs DFT adsorption energy of OH on different Perovskite structure.

Table 1ICOHP and ICOBI of Co-O atom pair close to the dopant atom.

| Surface dopant | ICOHP Pristine | Fe/P | Fe | P | ICOBI Pristine | Fe/P | Fe | P |
|----------------|-------------------|--------|--------|--------|-------------------|-------|-------|-------|
| Atom pair | Co-O | Co-O | Co-O | Co-O | Co-O | Co-O | Co-O | Co-O |
| Spin-up | -0.927 | -0.915 | -1.012 | -0.388 | 0.146 | 0.143 | 0.168 | 0.036 |
| Spin-down | -1.040 | -1.042 | -1.026 | -0.589 | 0.149 | 0.150 | 0.156 | 0.060 |

step. Furthermore, coupled with 1 e-, O* is attacked by hydroxyl anion to form the hydroperoxide intermediate OOH* in the third step and a further proton-coupled electron transfer in the fourth step releases O₂ and regenerates the free active site. Clearly, the adsorption and interaction of OH group is critical to facilitate the oxygen evolution. Researchers have suggested that the OER activity of oxides is correlated with the metal-OH bond strength [35,36], which supports our conclusion that metal-oxide covalency, particularly, transition metal e_g orbital hybridization with O 2p orbitals, can be the property descriptor for oxides' OER activity. To further confirm this correlation, DFT calculations were carried out to estimate the surface interactions of OH groups on different surfaces (Fig. 5& Table S6). Previous studies have shown a linear relationship between the adsorption energy of OH and OER performance of Perovskites [36-38]. Similarly, we observed that the experimental OER performance increases with decrease in the calculated adsorption energy of OH on the perovskite and OH stretching frequency (see Fig. 5a). The lowest adsorption energy of OH is on the LaCo_{0.92}Fe_{0.04}P_{0.04}O₃ perovskite. The lower adsorption energy enhances the first elementary reaction step (OH $^-$ + * \to OH* + e $^-$) of OER. Fig. 5b shows how the OER activity increases with lower OH stretching frequency (longer adsorbed OH bond length) and weaker OH bond making the second elementary reaction step (OH* + OH $^- \rightarrow$ O* + H₂O + e $^-$) of the OER easier to occur. This second elementary step involves shuttling of a hydrogen from the surface species to OH, forming H₂O in the solution and the weaker OH bond enhances that shuttling of H into the solution. The DFT results confirm the experimental trend that LaCo_{0.9}. Fe_{0.05}P_{0.05}O₃ has the best OER performance with the lowest overpotential, and the LaCo_{0.9}Fe_{0.1}O₃ shows the worst OER performance. This supports our claim that metal-oxygen hybridization between transition metal e_g orbitals and O 2p orbitals could be a good activity descriptor for OER.

The projected Crystal orbital Hamilton population (COHP) for the Co-O atom pair close to the dopant atom in the different surfaces is shown in the SI. (Fig. S13) [39,40] The integrated COHP (ICOHP) and Integrated crystal orbital bond index (ICOBI) are shown in Table 1. The ICOHP and ICOBI calculations indicate an increase in Co and O coupling with Fe doping while it remains similar with Fe and P co-dopants. However, the coupling strength decreased when doped with P only. This is in quantitative agreement with the TMOBC in Fig. 4b and c where Fe doped perovskite has the strongest metal-O bond strength, followed by Fe/P and P doped. (Table 1) ICOHP for La, Co, Fe, and P -O (H) atom

pair on the different surfaces are shown in the SI. (Table S7)

3. Conclusions

In summary, we have studied the role of metallic (Fe, Co) and nonmetallic (P) substitution to tune the OER catalytic performance of perovskites. We observed an increased OER catalytic activity with cosubstitution of P and Fe due to the change in TMOBC. Although no changes in catalyst structure and cation redox were observed, differences in metal-oxygen covalency were identified for these catalysts, which is the critical factor resulting in the different OER activities. Based on detailed surface-sensitive O K-edge XAS analysis, we propose that the greater transition metal e_g orbital hybridization with O 2p orbitals leads to higher OER performance, which combines the eg orbital theory and TMOBC theory in one new descriptor. Such correlation was confirmed by DFT calculation on the adsorption energy of OH on the perovskite and OH stretching frequency. This study provides deep insights into the effect of electronic structures on the OER kinetics and mechanisms, as well as guidance for the development of more active oxide catalysts for OER in the future.

Author contributions

M.W., and Z.F. conceived the project. M.W. and B. M. synthesized the materials and carried out the electrochemical measurements. K.C. carried performed DFT calculations. S.K. performed the COHP and COBI analysis. W. S carried out the *in-situ* XRD measurements. Z. H. and L.F. did the BET measurements. M. L. did the EDX and SEM measurements. M.W., C.C., A.C., and A.D. performed *ex-situ* soft XAS measurements and analysis. M.W., G.S., and Z.F. carried out the *in-situ* and operando XAS measurements and analysis. M.W., K.C., L.A., and Z. F. wrote the manuscript. All authors discussed the results and commented on the manuscript.

Declaration of Competing Interest

The authors declare that they have no known competing financial interests or personal relationships that could have appeared to influence the work reported in this paper.

Data availability

Data will be made available on request.

Acknowledgments

This work was financially supported by start-up funds from Oregon State University and National Science Foundation (NSF) under the contract no. CBET-1949870, CBET-2016192, CBET-2151049, DMR-1832803, CHE-1665287, and CBET 2223447. Part of this research was conducted at the Northwest Nanotechnology Infrastructure, a National Nanotechnology Coordinated Infrastructure site at Oregon State University which is supported in part by the National Science Foundation (Grant NNCI-2025489) and Oregon State University. W. S. S. acknowledges PNNL-OSU Distinguished Graduate Research Fellowship support by the U.S. Department of Energy (DOE), Office of Science, Office of Basic Energy Sciences, Division of Materials Sciences and Engineering under award no. 10122. The hard XAS measurements were done at beamline 9-BM of the Advanced Photon Source, which is a U.S. DOE Office of Science User Facility operated for the DOE Office of Science by National Laboratory under Contract AC02-06CH11357.The soft X-ray absorption spectroscopy measurements were performed at beamline 6.3.1 of Advanced Light Source, which is an Office of Science User Facility operated for the U.S. DOE Office of Science by Lawrence Berkeley National Laboratory and supported by the DOE under Contract No. DEAC02-05CH11231. Part of the DFT calculations used the Extreme Science and Engineering Discovery Environment (XSEDE)[40], through allocation TG-ENG170002 and TG-DMR160093, XSEDE is supported by National Science Foundation Grant No. ACI-1053575. The authors acknowledge the Texas Advanced Computing Center (TACC) at The University of Texas at Austin and the Comet cluster at the San Diego Supercomputer Center for providing HPC resources that have contributed to the research results reported within this paper.

Supplementary materials

Supplementary material associated with this article can be found, in the online version, at doi:10.1016/j.electacta.2023.143034.

References

- [1] X. Zhang, X. Zhang, H.M. Xu, Z.S. Wu, H.L. Wang, Y.Y. Liang, Iron-doped cobalt monophosphide nanosheet/carbon nanotube hybrids as active and stable electrocatalysts for water splitting, Adv. Funct. Mater. 27 (24) (2017) 06635.
- [2] U. De Silva, J. Masud, N. Zhang, Y. Hong, W.P.R. Liyanage, M.A. Zaeem, M. Nath, Nickel telluride as a bifunctional electrocatalyst for efficient water splitting in alkaline medium, J. Mater. Chem. A 6 (17) (2018) 7608–7622.
- [3] J.H. Kim, K. Kawashima, B.R. Wygant, O. Mabayoje, Y. Liu, J.H. Wang, C. B. Mullins, Transformation of a cobalt carbide (Co3C) oxygen evolution precatalyst, ACS Appl. Energy Mater. 1 (10) (2018) 5145–5150.
- [4] Y.K. Zhang, C.Q. Wu, H.L. Jiang, Y.X. Lin, H.J. Liu, Q. He, S.M. Chen, T. Duan, L. Song, Atomic iridium incorporated in cobalt hydroxide for efficient oxygen evolution catalysis in neutral electrolyte, Adv. Mater. 30 (18) (2018) 07522.
- [5] P.S. Li, M.Y. Wang, X.X. Duan, L.R. Zheng, X.P. Cheng, Y.F. Zhang, Y. Kuang, Y. P. Li, Q. Ma, Z.X. Feng, W. Liu, X.M. Sun, Boosting oxygen evolution of single-atomic ruthenium through electronic coupling with cobalt-iron layered double hydroxides, Nat. Commun. 10 (2019) 1711.
- [6] Y.L. Zhu, W. Zhou, J. Yu, Y.B. Chen, M.L. Liu, Z.P. Shao, Enhancing electrocatalytic activity of perovskite oxides by tuning cation deficiency for oxygen reduction and evolution reactions, Chem. Mater. 28 (6) (2016) 1691–1697.
- [7] Y. Duan, S.N. Sun, S.B. Xi, X. Ren, Y. Zhou, G.L. Zhang, H.T. Yang, Y.H. Du, Z.C. J. Xu, Tailoring the Co 3d-O 2p covalency in LaCoO3 by Fe substitution to promote oxygen evolution reaction, Chem. Mater. 29 (24) (2017) 10534–10541.
- [8] J. Suntivich, K.J. May, H.A. Gasteiger, J.B. Goodenough, Y. Shao-Horn, A perovskite oxide optimized for oxygen evolution catalysis from molecular orbital principles, Science 334 (6061) (2011) 1383.
- [9] Y.L. Zhu, W. Zhou, J. Sunarso, Y.J. Zhong, Z.P. Shao, Phosphorus-doped perovskite oxide as highly efficient water oxidation electrocatalyst in alkaline solution, Adv. Funct. Mater. 26 (32) (2016) 5862–5872.

- [10] W.H. Zhang, W.L. Zhou, Z.B. Zhang, Z.L. Chen, S.Z. Tan, D.J. Chen, Selective partial substitution of b-site with phosphorus in perovskite electrocatalysts for highly efficient oxygen evolution reaction, Chemnanomat 5 (3) (2019) 352–357.
- [11] Z.S. Li, L. Lv, J.S. Wang, X. Ao, Y.J. Ruan, D.C. Zha, G. Hong, Q.H. Wu, Y.C. Lan, C. D. Wang, J.J. Jiang, M.L. Liu, Engineering phosphorus-doped LaFeO3-delta perovskite oxide as robust bifunctional oxygen electrocatalysts in alkaline solutions, Nano Energy 47 (2018) 199–209.
- [12] K.A. Stoerzinger, L. Qiao, M.D. Biegalski, Y. Shao-Horn, Orientation-dependent oxygen evolution activities of rutile IrO2 and RuO2, J. Phys. Chem. Lett. 5 (10) (2014) 1636–1641.
- [13] M. Wang, Z. Feng, Pitfalls in X-ray absorption spectroscopy analysis and interpretation: a practical guide for general users, Curr. Opin. Electrochem. (2021), 100803
- [14] H.J. Tian, Z. Li, G.X. Feng, Z.Z. Yang, D. Fox, M.Y. Wang, H. Zhou, L. Zhai, A. Kushima, Y.G. Du, Z.X. Feng, X.N. Shan, Y. Yang, Stable, high-performance, dendrite-free, seawater-based aqueous batteries, Nat. Commun. 12 (1) (2021) 237.
- [15] C. Cai, M.Y. Wang, S.B. Han, Q. Wang, Q. Zhang, Y.M. Zhu, X.M. Yang, D.J. Wu, X. T. Zu, G.E. Sterbinsky, Z.X. Feng, M. Gu, Ultrahigh oxygen evolution reaction activity achieved using ir single atoms on amorphous CoOx nanosheets, Acs Catal. 11 (1) (2021) 123–130.
- [16] M.Y. Wang, L. Arnadottir, Z.C.,J. Xu, Z.X. Feng, In Situ X-ray absorption spectroscopy studies of nanoscale electrocatalysts, Nano Micro Lett. 11 (1) (2019) 47
- [17] J. Timoshenko, B.R. Cuenya, In Situ/operando electrocatalyst characterization by X-ray absorption spectroscopy, Chem. Rev. 121 (2) (2021) 882–961.
- [18] Z. Xiao, Y.C. Huang, C.L. Dong, C. Xie, Z. Liu, S. Du, W. Chen, D. Yan, L. Tao, Z. Shu, G. Zhang, H. Duan, Y. Wang, Y. Zou, R. Chen, S. Wang, Operando identification of the dynamic behavior of oxygen vacancy-rich Co3O4 for oxygen evolution reaction, J. Am. Chem. Soc. 28 (142) (2020) 12087–12095.
- [19] K.J. May, C.E. Carlton, K.A. Stoerzinger, M. Risch, J. Suntivich, Y.L. Lee, A. Grimaud, Y. Shao-Horn, Influence of oxygen evolution during water oxidation on the surface of perovskite oxide catalysts, J. Phys. Chem. Lett. 3 (22) (2012) 3264–3270.
- [20] M. Risch, A. Grimaud, K.J. May, K.A. Stoerzinger, T.J. Chen, A.N. Mansour, Y. Shao-Horn, Structural changes of cobalt-based perovskites upon water oxidation investigated by EXAFS, J. Phys. Chem. C 117 (17) (2013) 8628–8635.
- [21] V. Stamenkovic, B.S. Mun, K.J.J. Mayrhofer, P.N. Ross, N.M. Markovic, J. Rossmeisl, J. Greeley, J.K. Norskov, Changing the activity of electrocatalysts for oxygen reduction by tuning the surface electronic structure, Angew. Chem. Int. Ed. 45 (2006) 2897–2901.
- [22] J. Suntivich, H.A. Gasteiger, N. Yabuuchi, H. Nakanishi, J.B. Goodenough, Y. Shao-Horn, Design principles for oxygen-reduction activity on perovskite oxide catalysts for fuel cells and metal-air batteries, Nat. Chem. 3 (2011) 647.
- [23] M.W. Haverkort, Z. Hu, J.C. Cezar, T. Burnus, H. Hartmann, M. Reuther, C. Zobel, T. Lorenz, A. Tanaka, N.B. Brookes, H.H. Hsieh, H.J. Lin, C.T. Chen, L.H. Tjeng, Spin state transition in LaCoO3 studied using soft X-ray absorption spectroscopy and magnetic circular dichroism, Phys. Rev. Lett. 97 (2006), 176405.
- [24] Y. Kumagai, H. Ikeno, F. Oba, K. Matsunaga, I. Tanaka, Effects of crystal structure on Co-L(2,3) X-ray absorption near-edge structure and electron-energy-loss nearedge structure of trivalent cobalt oxides, Phys. Rev. B 77 (2008), 155124.
- [25] E.C. Wasinger, F.M.F. de Groot, B. Hedman, K.O. Hodgson, E.I. Solomon, L-edge X-ray absorption spectroscopy of non-heme iron sites: experimental determination of differential orbital covalency, J. Am. Chem. Soc. 125 (2003) 12894–12906.
- [26] P.S. Miedema, F.M.F. de Groot, The Iron L edges: fe 2p X-ray Absorption and Electron Energy Loss Spectroscopy, J. Electron Spectrosc. 187 (2013) 32–48.
- [27] M. Wang, B. Han, J. Deng, Y. Jiang, M. Zhou, M. Lucero, Y. Wang, Y. Chen, Z. Yang, A.T. N'Diaye, Q. Wang, Z.J. Xu, Z. Feng, Influence of Fe substitution into LaCoO3 electrocatalysts on oxygen-reduction activity, ACS Appl. Mater. Interfaces. 11 (6) (2019) 5682–5686.
- [28] F. Frati, M.O.J.Y. Hunault, F.M.F. de Groot, Oxygen K-edge X-ray absorption spectra, Chem. Rev. 120 (9) (2020) 4056–4110.
- [29] K. Sultan, M. Ikram, S. Gautam, H.K. Lee, K.H. Chae, K. Asokan, Electrical and magnetic properties of the pulsed laser deposited Ca doped LaMnO3 thin films on Si (100) and their electronic structures, RSC Adv. 5 (85) (2015) 69075–69085.
- [30] J. Suntivich, W.T. Hong, Y.L. Lee, J.M. Rondinelli, W. Yang, J.B. Goodenough, B. Dabrowski, J.W. Freeland, Y. Shao-Horn, Estimating hybridization of transition metal and oxygen states in perovskites from O K-edge X-ray absorption spectroscopy, J. Phys. Chem. C 118 (4) (2014) 1856–1863.
- [31] F. Song, L. Bai, A. Moysiadou, S. Lee, C. Hu, L. Liardet, X. Hu, Transition metal oxides as electrocatalysts for the oxygen evolution reaction in alkaline solutions: an application-inspired renaissance, J. Am. Chem. Soc. 140 (25) (2018) 7748–7759.
- [32] N.T. Suen, S.F. Hung, Q. Quan, N. Zhang, Y.J. Xu, H.M. Chen, Electrocatalysis for the oxygen evolution reaction: recent development and future perspectives, Chem. Soc. Rev. 46 (2) (2017) 337–365.
- [33] H. Dau, C. Limberg, T. Reier, M. Risch, S. Roggan, P. Strasser, The mechanism of water oxidation: from electrolysis via homogeneous to biological catalysis, ChemCatChem 2 (7) (2010) 724–761.
- [34] J.O.M. Bockris, Kinetics of activation controlled consecutive electrochemical reactions: anodic evolution of oxygen, J. Chem. Phys. 24 (4) (1956) 817–827.
- [35] C.G. Morales-Guio, L. Liardet, X. Hu, Oxidatively electrodeposited thin-film transition metal (Oxy)hydroxides as oxygen evolution catalysts, J. Am. Chem. Soc. 138 (28) (2016) 8946–8957.
- [36] J.O.M. Bockris, T. Otagawa, The electrocatalysis of oxygen evolution on perovskites, J. Electrochem. Soc. 131 (2) (1984) 290–302.

- [37] S. Zhao, L.T. Yan, H.M. Luo, W. Mustain, H. Xu, Recent progress and perspectives of bifunctional oxygen reduction/evolution catalyst development for regenerative anion exchange membrane fuel cells, Nano Energy 47 (2018) 172–198.
- [38] E. Fabbri, A. Habereder, K. Waltar, R. Kotz, T.J. Schmidt, Developments and perspectives of oxide-based catalysts for the oxygen evolution reaction, Catal. Sci. Technol. 4 (11) (2014) 3800–3821.
- [39] R. Dronskowski, P.E. Blochl, Crystal orbital hamilton populations (Cohp) energy-resolved visualization of chemical bonding in solids based on density-functional calculations, J. Phys. Chem. 97 (33) (1993) 8617–8624. Us.
- [40] J. Towns, T. Cockerill, M. Dahan, I. Foster, K. Gaither, A. Grimshaw, V. Hazlewood, S. Lathrop, D. Lifka, G.D. Peterson, XSEDE: accelerating scientific discovery, Comput. Sci. Eng. 16 (5) (2014) 62–74.